

# Minimal spanning trees at the percolation threshold: a numerical calculation

Sean M. Sweeney and A. Alan Middleton

*Department of Physics, Syracuse University, Syracuse, NY 13244, USA*

The fractal dimension of minimal spanning trees on percolation clusters is estimated for dimensions  $d$  up to  $d = 5$ . A robust analysis technique is developed for correlated data, as seen in such trees. This should be a robust method suitable for analyzing a wide array of randomly generated fractal structures. The trees analyzed using these techniques are built using a combination of Prim's and Kruskal's algorithms for finding minimal spanning trees. This combination reduces memory usage and allows for simulation of larger systems than would otherwise be possible. The path length fractal dimension  $d_s$  of MSTs on critical percolation clusters is found to be compatible with the predictions of the perturbation expansion developed by T. S. Jackson and N. Read [T. S. Jackson and N. Read, Phys. Rev. E **81**, 021131 (2010)].

## I. INTRODUCTION TO THE PROBLEM

The statistical physics and dynamics of disordered physical systems naturally leads to the study of fractal geometric objects. Physical systems with quenched disorder, i.e., those with fixed random heterogeneities, often have power law correlations at large scales or interfaces that are fractal or self-affine. These structures can result from some global optimization problem that has connections with graph theory. For example, Dijkstra's shortest path algorithm [1, 2] can be used to find the lowest energy path of a vortex line in a disordered superconductor [3, 4], and these paths are self-affine. Excitations in a disordered XY model in two dimensions [5, 6], domain walls in spin glasses [7], and boundaries between drainage basins [8] are examples of physical objects with fractal dimension that are found by global optimization.

A structure with fractal scaling that arises in physical contexts is the minimal spanning tree (MST). One such context is a highly disordered Ising spin glass. Newman and Stein showed that for the strongly disordered limit, the problem of finding a ground state can be directly mapped to finding an MST [9]. This mapping can be used to investigate the multiplicity of ground states in the thermodynamic limit. Minimal spanning trees have other applications such as in transportation networks connecting cities [10], telecommunications networks connecting remote computer terminals [11], efficient circuit design [12], taxonomic reconstruction of evolutionary trees [13], and pattern recognition in image analysis [14].

A minimal spanning tree is a structure that connects a set of nodes with minimum total cost. This structure is defined for a weighted graph  $G = (V, E, w)$  where  $V$  is a set of vertices (or nodes),  $E$  is a set of edges that connect vertices, and  $w$  is a weight function, with each edge  $e \in E$  having weight  $w(e)$ . A spanning tree is a loopless connected set of edges that includes all the vertices in  $V$ . The minimal spanning tree is the spanning tree  $T$  that minimizes the total weight

$$w(T) = \sum_{e \in T} w(e). \quad (1)$$

This is a well-known problem in computer science and

combinatorics. See Ref. [15] for a general overview of MSTs and MST-finding algorithms.

A notable fact about the MST is that the minimal tree is determined only by the numerical ordering of the weights, i.e., it is otherwise independent of their value. So there is a large invariance or universality for these structures; their geometry is independent of the disorder distributions. As long as the weights  $w(e)$  are independently drawn from the same distribution (independent identically distributed or i.i.d. weights), the edges can be sorted in order of increasing weight. This ordering alone determines the tree. Two physical problems with wholly different distributions of quenched disorder have MSTs with equivalent statistics.

Recently, Jackson and Read carried out an analytical calculation for the fractal dimension  $d_s$  of paths in MSTs [16, 17]. They developed a perturbation expansion for  $d_s$  for MSTs on critical percolation clusters in  $d$  dimensions, obtaining the result

$$d_s = 2 - \frac{\epsilon}{7} + \mathcal{O}(\epsilon^2), \quad (2)$$

where  $\epsilon = 6 - d$  and  $d = 6$  is the upper critical dimension [17]. In general, disordered systems are difficult to analyze and rarely yield quantitative analytic results. This prediction therefore provides a strong motivation for more precise computation of fractal dimensions in spanning trees, in particular, dimensions of the trees on spanning percolation clusters. We note that it is unclear whether the fractal dimension of these trees is affected by being constructed on spanning percolation clusters as opposed to a whole lattice. The work presented in this paper seeks to numerically compute  $d_s$  in dimensions  $2 \leq d \leq 5$  for comparison with Eq. (2). This calculation employs a combination of memory-saving techniques to simulate large systems as well as careful data fitting procedures to obtain precise estimates for  $d_s$  in the limit of infinite system size.

Our final calculations for  $d_s$  yield values of 1.216(1) for  $d = 2$ , 1.46(1) for  $d = 3$ , 1.65(2) for  $d = 4$ , and 1.86(4) for  $d = 5$  (refer to Table I). We develop and utilize a  $\chi^2$  test that accounts for the scale-invariant correlations found in the data, allowing for an improved  $\chi^2$  measure and robust estimates of the uncertainty in the effective

exponent at scale  $L$ ,  $d_s(L)$ . We then use linear and non-linear least squares fitting to extrapolate to the infinite system size limit. We find the numerical results to be of higher precision than previous calculations and compatible with Eq. (2), though more conclusive confirmation requires improved numerical statistics and higher order analytic work. We emphasize that the analysis procedure used here is generalizable and could be useful for other work dealing with disordered systems.

## II. MODEL & ALGORITHMS

To model MSTs on percolation clusters, we simulated hypercubic lattices with  $L$  vertices per side with periodic boundary conditions, giving  $L^d$  total vertices and  $dL^d$  total edges. Edges are independently given a weight randomly distributed on the interval  $(0, 1)$ , where  $w(e)$  is represented by a double precision number. Very rarely two edges are assigned the same weight. In this case, a new random weight is generated for one of these edges until a weight is generated that does not match any previously assigned weight. An important distinction to note is that rather than seeking to find a tree that spans all of the vertices in these hypercubic lattices, we seek to find the MST on a percolation cluster that wraps around the periodic lattice (in any of the  $d$  directions) at the threshold of percolation. Thus the MST-finding algorithms are stopped when the tree contains a subset of vertices that wraps around the system instead of including all  $L^d$  vertices of the graph. The final object of interest, the MST on a critical percolation cluster, contains only a small subset of the set of vertices  $V$  in the lattice.

In order to avoid confusion, we first note a dual usage of the term spanning. For an MST, spanning means that the tree includes all vertices in the graph for which the MST is found. In the context of percolation theory, the term refers to a cluster that is spanning or percolating around the lattice. We use spanning in both senses, with the correct sense implied by the context.

One naive approach to finding the MST on a graph is to iterate through the list of all spanning trees and select the tree with the lowest total weight. This approach might work on a small finite graph, but the number of trees grows exponentially with  $L^d$ . In order to analyze properties of MSTs in the thermodynamic limit of infinite system size, a more efficient MST-finding algorithm (both in terms of running time and maximum memory requirements) is needed.

As background for the algorithms used to find MSTs, it might be helpful to briefly review the relationship between invasion percolation and Bernoulli percolation. In Bernoulli (bond) percolation [18, 19], edges in a random graph have a probability  $p$  to be occupied, and a probability  $1 - p$  to be unoccupied. After determining the occupation of each edge independently, one inspects the graph to check for long-range connectivity in the form of a cluster of connected vertices that percolates, i.e., spans

the graph. On a periodic hypercubic lattice, one definition of a percolating or spanning cluster is a cluster that wraps around the lattice along one or more of the  $d$  spatial dimension axes. Such a cluster contains a loop that cannot be contracted to a point.

Examining larger and larger systems on a macroscopic scale, this percolation transition becomes clear; below some critical percolation probability  $p_c$  only small clusters are seen, but at  $p = p_c$  large clusters that span the system begin to emerge. Aizenman refers to these large critical clusters as incipient spanning clusters (ISCs), a term which is closely related to, but distinct from, the incipient infinite cluster (IIC) [20, 21]. In the exploration of Bernoulli percolation, this occupation probability  $p$  is finely tuned in order to observe this critical transition and the clusters that are formed at criticality.

An alternate approach to percolation is invasion percolation [22]. Invasion percolation is a procedure that greedily occupies edges of low weight  $w$  and has a termination condition. Invasion percolation consists of a growing cluster  $C$  that is a subset of  $E$ . This cluster has a set of adjacent edges  $\partial C$ . The cluster  $C$  begins as a single occupied seed site. Additional sites are “invaded” by choosing from  $\partial C$  the lowest weight edge,  $e_l(\partial C)$  and expanding the invaded region to include this edge, by adding  $e_l(\partial C)$  to  $C$ . This invasion percolation process can be repeated until long-range connectivity is observed (i.e., until the invaded region percolates across the system).

There has been much discussion [23–25] on how to relate the clusters of invasion percolation to those of ordinary Bernoulli percolation. There seems to be a strong reason to believe that in the limit of infinite system size, infinite connected clusters created using both of these percolation methods should obey the same scaling relations, meaning that the fractal path length dimension  $d_s$  should be the same for both methods. Invasion percolation is extremely useful because it allows for the simulation of critical percolation systems without having any knowledge of what the value of  $p_c$  is for a particular system. Thus invasion percolation is an example of self-organized criticality [23, 24].

In our particular case, we’re interested in analyzing the MSTs that lie on an ISC. In other words, we want to find the MST for the ISC. We’ll refer to this final object as the MTISC (minimal tree for an incipient spanning cluster). Here we use two algorithms, Kruskal’s algorithm [26] and Prim’s algorithm [10]. While Prim’s algorithm is similar to the invasion percolation process described above [27], Kruskal’s algorithm is related to Bernoulli percolation due to the global nature of the algorithm. However, neither algorithm actually requires the choice of an occupation probability  $p$  as a parameter, and consequently both processes exhibit self-organized critical behavior, as the growth is stopped when a tree is found that wraps [28]. For a more precise definition of these algorithms, refer to Appendix A. We next present less formal descriptions of these algorithms.

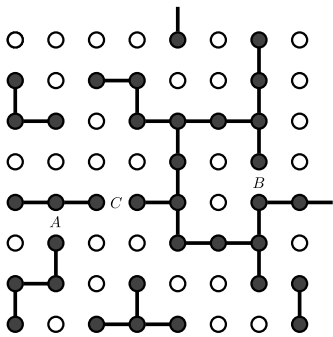


Figure 1: A sample iteration of Kruskal's algorithm on an eight by eight periodic square lattice ( $d = 2$ ). At a given step, the state is a forest of trees, which includes isolated sites (open circles) and larger trees (connected solid circles). During each step of the algorithm, the edge with the lowest weight is selected from the remaining unselected edges. For example, if edge  $A$  is selected, the trees containing either endpoint of edge  $A$  are merged into a single tree. If edge  $B$  is selected, its addition would form a non-wrapping loop (forbidden cycle), so edge  $B$  is not added to any tree and is removed from future consideration. If edge  $C$  is selected, its addition would form a wrapping loop (allowed cycle), so the algorithm is terminated. The tree containing the endpoints of edge  $C$  is then the Kruskal's MTISC,  $T_K$ .

### A. Kruskal's algorithm

Kruskal's algorithm is an MST-finding algorithm that considers all edges of a graph. In Kruskal's algorithm, we grow a forest of many small trees, merging small groups of trees into larger trees and eventually identifying one of these large trees as the MTISC, terminating the algorithm. At the start of Kruskal's algorithm, each vertex is its own isolated tree. All of the edges that are not yet part of a tree are sorted, and the edge with minimal weight is selected, excluding edges that would form non-wrapping loops. When an edge is selected, the trees containing each of its vertices are joined into a single tree. This process continues until a tree grows big enough that it wraps around the periodic lattice. At this time, this tree is identified as the Kruskal's MTISC,  $T_K$ . This process is illustrated in Fig. 1.

Kruskal's algorithm bears similarity to Bernoulli percolation in that it is a non-local algorithm that requires information about all edges of the graph. If we consider a graph with edges whose weights are distributed evenly on  $(0, 1)$  and run Kruskal's algorithm until we first examine an edge with weight  $w > p_c$ , the sites of  $T_K$  are identical to those obtained from performing Bernoulli percolation on the same graph with occupation probability  $p_c$ .

### B. Prim's algorithm

Prim's algorithm is equivalent to algorithms for loop-less invasion percolation [27]. At the start of the algo-

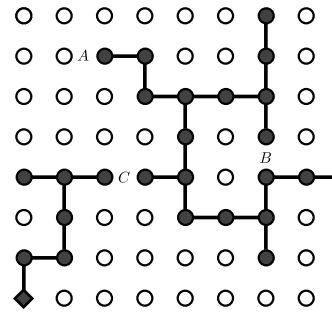


Figure 2: A sample iteration of Prim's algorithm on an eight by eight periodic square lattice ( $d = 2$ ). The tree is represented by connected solid circles and lines, while unoccupied sites are shown as open circles. The diamond-shaped vertex at the bottom left of the lattice is the initial seed site  $v_0$ . During each step of the algorithm, the edge adjacent to the current Prim's tree with the lowest weight is selected. If edge  $A$  is selected, it is added to the Prim's tree, along with the endpoint of  $A$  that is not already in the Prim's tree. If edge  $B$  is selected, its addition to the Prim's tree would form a non-wrapping loop (forbidden cycle), so edge  $B$  is not added to the tree and is removed from future consideration. If edge  $C$  has the lowest weight and is selected, its addition would cause the Prim's tree to wrap around the periodic lattice (adding an allowed cycle), so the algorithm is terminated, leaving the current Prim's tree as the Prim's MTISC,  $T_P$ .

rithm, the MST consists of a single seed site. This tree grows outward from this vertex through the examination and conditional addition of adjacent edges, as edges adjacent to the growing tree are examined. At any given iteration, the minimal weight adjacent edge is selected and incorporated into the tree, excluding edges that would lead to non-wrapping loops. The check for which edges form a loop is simple: if both ends of the edge are in the current tree a loop would be formed. To check whether a loop is wrapping or non-wrapping, the algorithm assigns to each vertex  $a$  a displacement  $\vec{r}_a$  from the origin. This displacement is found for a newly added vertex  $b$  by adding a vector displacement  $\vec{e}_{ab}$  for the edge to the vector displacement of the end of the edge (site) that is already in the tree  $\vec{r}_a$ . Thus for a newly added site  $b$  we have  $\vec{r}_b = \vec{r}_a + \vec{e}_{ab}$ . When a loop is encountered, this new site  $b$  will already have a vector displacement  $\vec{r}'_b$  defined, since this site is already in the tree. If the relative displacement  $|\vec{r}_b - \vec{r}'_b|$  between these two labelings is greater than  $L$ , the loop formed is a wrapping loop. When this wrapping edge is examined, the algorithm is terminated, and this final tree is identified as the Prim's MTISC,  $T_P$ , as shown in Fig. 2.

To increase efficiency when generating MTISCs, Kruskal's and Prim's algorithms can be engineered to save memory by creating edges and weights only as needed during the execution of the growth algorithm rather than at the start [29, 30]. The memory saved in the Prim's method is much larger and leads to an overall more memory efficient method because Prim's algorithm only requires the growing of a single tree rather than a

large forest of trees. Due to this decreased memory usage, it is possible to simulate larger systems with Prim's algorithm than with Kruskal's algorithm.

### C. Two-step method

We used a two-step method, combining Prim's and Kruskal's algorithms in order to take advantage of the increased efficiency afforded by Prim's algorithm when selecting a typical MTISC. We first generate a tree  $T_P$  using Prim's algorithm and then apply Kruskal's algorithm to this tree, ensuring that the MTISC obtained has the same scaling as the MTISC that would be obtained by increasing  $p$  large enough to form a forest, one of whose trees is the final tree  $T_K$ . The data presented in this paper comes from analysis of MTISCs generated by the two-step method, as well as comparisons with the intermediate data from  $T_P$ , before Kruskal's algorithm is applied to  $T_P$ .

While Prim's algorithm in general takes less time and memory to find an MTISC than Kruskal's algorithm, the two algorithms do not find exactly the same MTISC [31]. As shown in detail in Appendix B, either  $T_K$  is a subset of  $T_P$ , or they do not intersect. We are interested in constructing an MTISC that is either identical to  $T_K$  or scales the same as  $T_K$ . The non-local greedy edge selection of Kruskal's algorithm guarantees  $T_K$  to have the same sites as a Bernoulli percolation cluster.

A technical detail to note about the two-step method is that in the final stage of Prim's algorithm when a wrapping edge is selected, we add this edge to the final Prim's tree  $T_P$ . This is done so that when Kruskal's algorithm is applied to  $T_P$ , there will be a wrapping edge to satisfy the termination condition of Kruskal's algorithm. While the inclusion of this edge temporarily destroys the tree-like nature of  $T_P$ , its inclusion is essential.

Because Prim's growth begins at a random seed site that does not necessarily belong to  $T_K$ , often the  $T_K$  is a subset of  $T_P$ . This of course depends which vertex  $v_0$  is used as the seed site for Prim's growth, as the Prim's MTISC is a function of its seed site,  $T_P(v_0)$ . Executing Kruskal's algorithm in the second step of this method serves to "trim off" the part of  $T_P(v_0)$  that includes the seed site  $v_0$  and that does not belong to  $T_K$ . The tree derived from this procedure is termed the two-step MTISC,  $T_2$ . This method is illustrated in Fig. 3.

We show in Appendix B that this two-step procedure yields the Kruskal's MTISC, i.e.,  $T_2 = T_K$ , in all cases except when there naturally arise multiple disjoint ISCs on the lattice at criticality. By direct simulation of these systems, we observed that  $T_2 \neq T_K$  about 0.2% of the time in two dimensions, 1% in three dimensions, and 5% in four dimensions. Five dimensional samples were not compared due to the large memory demands of simulating minimal spanning forests in five dimensions.

We suppose by standard scaling that in the case where  $T_2 \neq T_K$ ,  $T_2$  and  $T_K$  should have the same scaling prop-

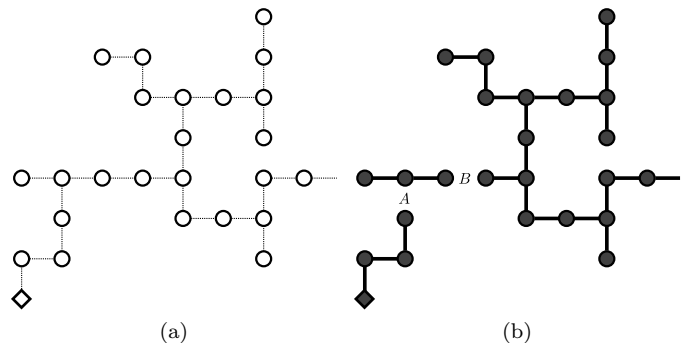


Figure 3: Illustration of the two-step method. This method grows a candidate MTISC using the Prim's method and then trims the tree using Kruskal's algorithm. (a) depicts  $T_P$  (plus the final wrapping edge) which is given as input to Kruskal's algorithm. During construction of this tree, only edges adjacent to the tree are tested. The potential connectivity of the unoccupied sites is explicitly shown using open circles and thin lines, and for reference the Prim's seed site  $v_0$  at the bottom left of the lattice is represented by a diamond. (b) shows the state of the graph after running 23 steps of Kruskal's algorithm on  $T_P$ , with trees being represented by connected solid circles. If edge  $B$  is selected before edge  $A$ , i.e.,  $w(B) < w(A)$ , the Prim's seed site  $v_0$  will not be part of  $T_K$ , and the disconnected portion of the graph containing the Prim's seed site  $v_0$  will be trimmed off.

erties. We have simulated some samples in this case for systems up to size  $512^2$ ,  $64^3$ , and  $32^4$  and observed similar scaling properties between  $T_2$  and  $T_K$ . The memory requirements for the two-step method allowed us to simulate systems of size  $2048^2$  within roughly 2GB of memory,  $256^3$  within 1.5GB,  $64^4$  within 1GB, and  $48^5$  within 2GB.

## III. ANALYSIS/METHODS

### A. Methods for scaling analysis

To find the fractal dimension of the minimal trees on spanning percolation clusters, we compute the Euclidean distance  $r$  and path length  $s$  between some origin on the MTISC and other points on the MTISC. Accurately determining the scaling in the limit of large clusters requires taking into account lattice effects, finite size effects, and statistical uncertainties. Given any two points on a tree, there is a unique path between the two points, so that the path length is easily defined. The choice of endpoints for the paths is chosen in a natural fashion for each tree.

For trees constructed using Prim's algorithm, the origin is taken to be the seed site where cluster growth begins. The set of paths connecting the origin to all other points in the tree is used in the statistics. For each tree  $T_P$ , we find  $n_P(s)$ , the number of paths of length  $s$  that start at the origin. We use  $r_P(s)$  to indicate the average over all paths of length  $s$  of the Euclidean distance  $|\vec{r}|$ .

After then running Kruskal’s algorithm on the Prim’s tree to find the trimmed MTISC  $T_2$ , a random origin is chosen on the trimmed tree. All paths from this new origin are used to find both  $r(s)$  and  $n(s)$ , the averaged Euclidean distance and number of paths. In order to reduce the amount of data stored, the full set of  $N$  samples is grouped into sets of  $N_b$  batches of uniform size  $N/N_b$ . The batch-averaged quantities of  $r(s)$  and  $n(s)$  for these trimmed trees are calculated and stored. Here we use  $r(s)$  and  $n(s)$  to refer to data generated by the two-step algorithm. As a comparison, we also looked at the averages for Prim’s trees, before trimming.

We assume that the paths on the tree are well described as fractal. The scaling of the sample-averaged  $r(s)$  will then follow the relation

$$r(s) \sim s^{1/d_s} . \quad (3)$$

If we write  $L$  as the length of one side of a hypercubic system, then  $s/L^{d_s}$  is a natural scaling parameter, and we expect to see finite size effects near  $s/L^{d_s} = 1$ , as paths of this length approach the size of the system. The standard one parameter finite size scaling assumption is then that  $r(s)$  will scale like  $s^{1/d_s}$  multiplied by some unknown function of the argument  $s^{1/d_s}L^{-1}$ . The form of the scaling hypothesis is that

$$\begin{aligned} r(s) &\approx s^{1/d_s} f\left(\frac{s^{1/d_s}}{L}\right) \\ &\approx s^{1/d_s} g\left(\frac{s}{L^{d_s}}\right) , \end{aligned} \quad (4)$$

where the scaling functions  $f(\omega)$  and  $g(\omega)$  behave as  $f(\omega) \approx c_1$  for some constant  $c_1$  for  $\omega \ll 1$ ,  $f(\omega) \approx 0$  as  $\omega \rightarrow \infty$ ,  $g(\omega) \approx c_2$  for some constant  $c_2$  for  $\omega \ll 1$ ,  $g(\omega) \approx 0$  as  $\omega \rightarrow \infty$ . For more compact formulas, we define the scaled dimensionless variables

$$\rho = \frac{r(s)}{s^{1/d_s}} , \quad (5)$$

$$\omega = \frac{s}{L^{d_s}} . \quad (6)$$

Using this scaling hypothesis, we can make estimates for  $d_s$  by plotting data for multiple system sizes on the scaled axes of  $\rho$  vs.  $\omega$ . If we tune the parameter  $d_s$ , we see that the curves for various sizes  $L_i$  can be made to collapse well near an estimated best value of  $d_s$  (see Fig. 4). While this method allows us to get a fair idea of this exponent  $d_s$ , it relies on subjective estimations of curve collapse and for that reason is not ideal when attempting precise estimates.

To have a better estimate for  $d_s$  and to estimate the uncertainty in this estimate, we have implemented an automated fitting procedure. This procedure determines an effective exponent  $d_s(L)$  derived from data for samples of size  $L$  and of larger size  $2L$  by minimizing a “goodness of fit” parameter  $\chi^2$  at each scale  $L$ . The only input

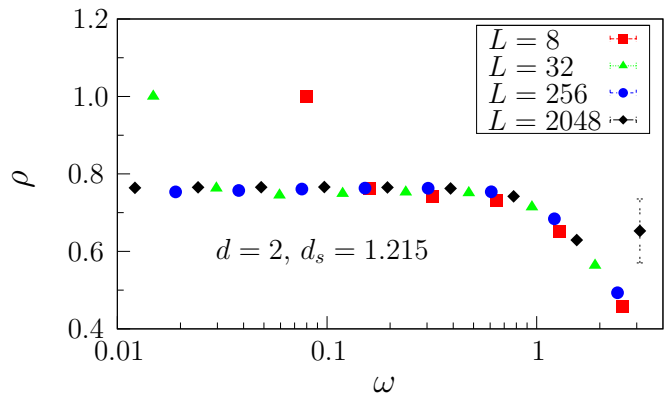


Figure 4: Scaling collapse for  $d = 2$  with  $d_s = 1.215$ , which appears to be moderately close to the true value of  $d_s$  judging by eye from the goodness of the collapse. Note that error bars are smaller than the symbol size for all points except the right-most point.

to this procedure is an estimate of  $s_l$ , the small path data cutoff, which is discussed in Appendix C. We then extrapolate  $d_s(L)$  for  $L \rightarrow \infty$  to get our best estimate for  $d_s$ .

The key part of this calculation is to choose a robust and reliable measure for  $\chi^2$ . This allows us to quantitatively measure how well the data for a given pair of system sizes collapses as a function of the parameter  $d_s$ . We seek a value of  $d_s$  for which this  $\chi^2$  is minimized (Fig. 5), though the magnitude of our final error bars are determined by resampling. Our definition of  $\chi^2$  must allow for non-uniform correlations in fluctuations of  $r(s)$  between different values of  $s$ , discrete lattice effects (small  $s$  lower data cutoff), and statistical uncertainties (large  $s$  upper data cutoff).

## B. Correlations in $r(s)$

In order to define a useful  $\chi^2$  statistic, we first focus on the correlations we observed in the  $r(s)$  data for the spanning trees. In summary, we find that these correlations have a range in  $s$  that grows linearly with increasing path length  $s$ , in dimensions  $d = 2, 3, 4, 5$ . We then modify the standard  $\chi^2$  test for uncorrelated data to account for these correlations.

To describe correlations in the averaged  $r(s)$  data, it will be helpful to first define how our data is averaged over samples, since we use multiple groupings of data for calculating averages. Let  $r_i(s)$  denote an average of Euclidean distance  $r = |\vec{r}|$  over all points on tree  $i$  that are at a chemical (path length) distance  $s$  from the origin for each tree  $i = 1, \dots, N$  in the  $N$  samples. For faster analysis, the  $N$  samples are organized into  $N_b$  batches. The batch index  $\alpha$  ranges over  $1 \leq \alpha \leq N_b$ . We will use  $r_\alpha(s)$  to denote an average over the  $m = N/N_b$  samples

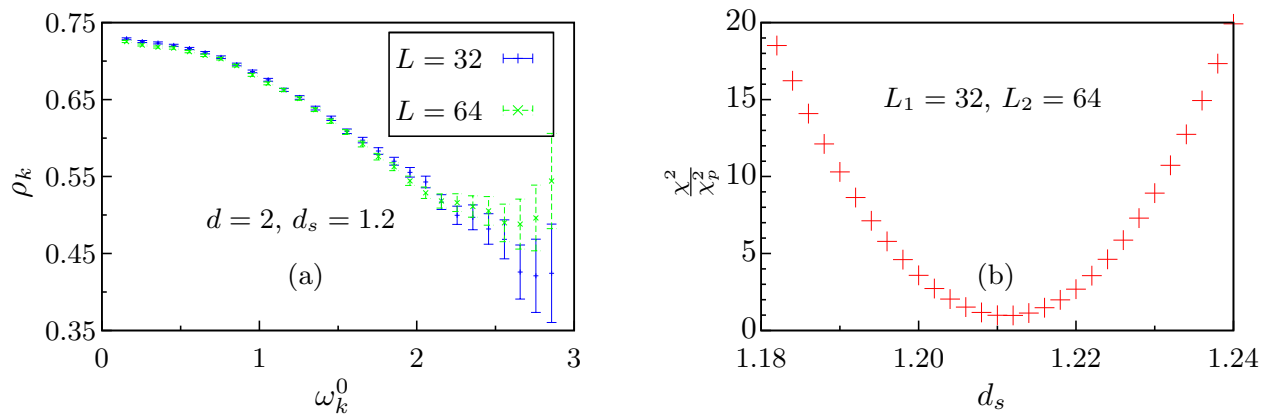


Figure 5: A sample collapse for two systems of size  $L = 32$  and  $L = 64$  in dimension  $d = 2$ . (a) Shows the comparison of the two systems at interpolated points  $\omega_k^0$  for a value of  $d_s = 1.2$ . Comparing the value of  $\rho_k(L_1 = 32)$  and  $\rho_k(L_2 = 64)$  at each of these points allows for the calculation of  $\chi^2(d_s; L_1, L_2)$ . (b) Shows  $\chi^2$  compared with an expected estimate  $\chi_p^2$  as a function of the fitting parameter  $d_s$  for the same pair of systems. Though we determine final error bars by resampling, the  $\chi^2$  model is shown for comparison.

in batch  $\alpha$ :

$$r_\alpha(s) = \frac{1}{m} \sum_{i \in \alpha} r_i(s). \quad (7)$$

The global average over all  $N$  samples will be represented by

$$\overline{r(s)} = \frac{1}{N_b} \sum_{\alpha=1}^{N_b} r_\alpha(s) = \frac{1}{N} \sum_{i=1}^N r_i(s). \quad (8)$$

To initially examine correlations over  $s$  of  $r_i(s)$  within a single tree, we plot the fluctuations of the batch averages  $r_\alpha(s)$  about the global average  $\overline{r(s)}$ . That is, we plot the variations of the average  $\delta r_\alpha(s)$ , where

$$\delta r_\alpha(s) = r_\alpha(s) - \overline{r(s)}, \quad (9)$$

vs. path length  $s$ . Fig. 6 displays these correlations for a typical batch of data in a system of size  $64^2$ .

Note that the form of the correlations should be independent of batch size, up to a multiplicative scaling factor. We can see this explicitly by examining  $\delta r_\alpha(s)\delta r_\alpha(t)$  for path length values  $s$  and  $t$ . For  $i \neq j$ ,  $i$  and  $j$  are independent samples, so we can use the relation

$$\overline{\delta r_i(s)\delta r_j(t)} = \overline{\delta r_i(s)} \overline{\delta r_j(t)} \quad (10)$$

and of course

$$\overline{\delta r_i(s)} = \overline{r_i(s) - \overline{r(s)}} = 0. \quad (11)$$

By standard computation all of the  $i \neq j$  cross terms are zero, and we are left with

$$\overline{\delta r_\alpha(s)\delta r_\alpha(t)} = \frac{1}{m} \overline{\delta r_i(s)\delta r_i(t)}, \quad (12)$$

showing that the choice of grouping the data into batches should not affect the form of the correlations in  $r(s)$ .

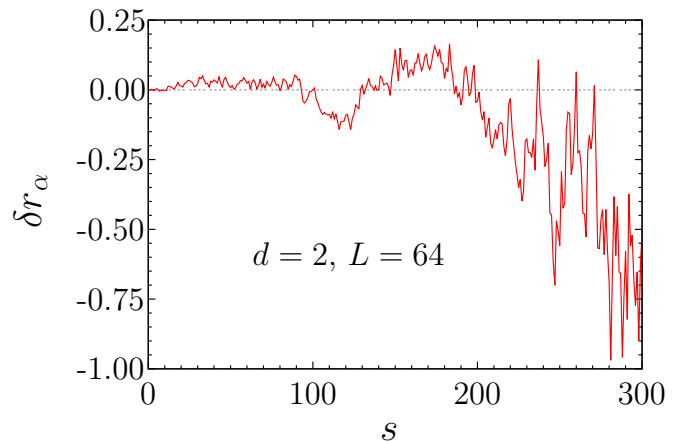


Figure 6: Variations from the mean for a typical batch  $\alpha$  of data for a system of size  $L = 64$  in dimension  $d = 2$ . The difference between the mean Euclidean distances  $\delta r_\alpha(s) = r_\alpha(s) - \overline{r(s)}$  is plotted vs. path length  $s$ .

To quantitatively examine these correlations we compute the correlation matrix  $c_{s,t}$  defined as

$$c_{s,t} = \frac{1}{N_b} \sum_{\alpha=1}^{N_b} \frac{\delta r_\alpha(s)\delta r_\alpha(t)}{\gamma(s)\gamma(t)}. \quad (13)$$

Here  $\gamma(s)$  is the root mean square fluctuation in  $\delta r_\alpha(s)$  computed over the  $N_b$  batches of data and is used to normalize the entries  $c_{s,t}$  of the correlation matrix:

$$\gamma^2(s) = \frac{1}{N_b} \sum_{\alpha=1}^{N_b} \delta r_\alpha^2(s). \quad (14)$$

A sample correlation matrix for  $L = 64$  is plotted in Fig. 7. The data suggests that the correlation length increases with increasing  $s$ . To construct a model for the

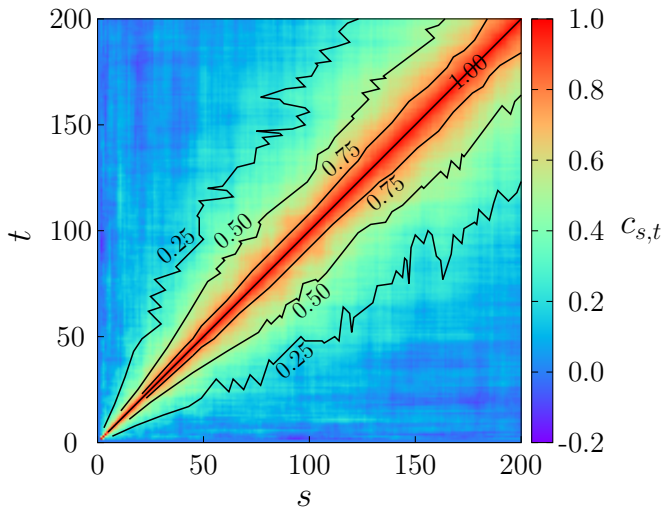


Figure 7: Correlation matrix  $c_{s,t}$  averaged over all data for systems of size  $L = 64$  in dimension  $d = 2$ . Selected contours are shown.

scaled correlation length, we measured the width along the diagonal of the peak in the correlation matrix for various values of  $s$ . We used different measures for measuring this width, including a measure of the full width at half maximum (how many “steps” away from the diagonal before  $c_{s,t}$  falls to a value of  $1/2$ ), a measure of one decay length (how many steps from the diagonal until  $c_{s,t}$  drops to a value of  $1/e$ ), and a measure using an exponential decay model  $c_{s,t} = \exp(-|s-t|/\ell')$  assuming an unscaled correlation length  $\ell'$ . We calculate  $\ell'$  using the zeroth moment of  $c_{s,t}$ , allowing us to then obtain the scaled correlation length  $\ell = \ell'/L^{d_s}$ , given a rough estimate for  $d_s$ .

Fig. 8 shows the scaled correlation length  $\ell$  vs.  $\omega$  for multiple system sizes for dimension  $d = 2$ , using the exponential decay model  $c_{s,t} = \exp(-|s-t|/\ell')$  for the unscaled correlation length  $\ell'$ . We see that  $\ell$  increases linearly with  $\omega$  up until roughly  $\omega = 1$ , at which point the scaled correlation length levels off to a constant value. Although the proportionality constant differs depending on which method is used to measure the correlation length, we observed a linear relationship between  $\ell$  and  $\omega$  in all cases. We also find this linearity in dimensions  $d = 2, 3, 4, 5$ . Based on this empirical observation, we choose an ansatz for the scaled correlation length.

$$\ell(\omega) \propto \begin{cases} \omega & : \omega \leq 1 \\ 1 & : \omega > 1 \end{cases} \quad (15)$$

For the exponential decay model used in Fig. 8, the proportionality is  $\ell \approx 0.24\omega$ . Physically, this means that on average, for any given growing path in a spanning tree, the path must grow about 24% longer than its current length before the correlations in the  $r(s)$  data for this path decay, using the exponential decay model  $c_{s,t} = \exp(-|s-t|/\ell')$  for the unscaled correlation length  $\ell'$ .

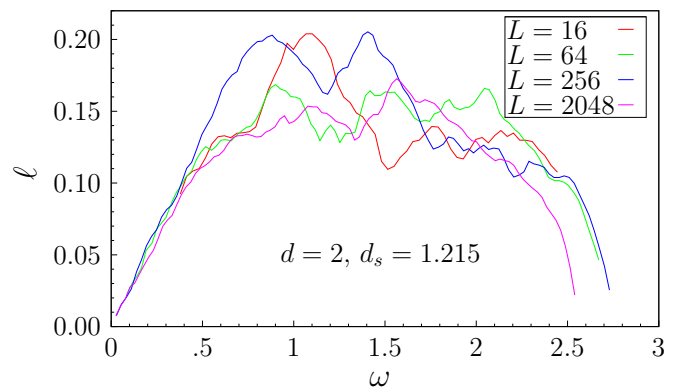


Figure 8: Scaled correlation length  $\ell$  vs.  $\omega$  for various systems in dimension  $d = 2$  with  $d_s = 1.215$ . In this case  $\ell$  was measured using the exponential decay model  $c_{s,t} = \exp(-|s-t|/\ell')$  for the unscaled correlation length  $\ell'$ , with the relation to the scaled correlation length  $\ell$  being  $\ell = \ell'/L^{d_s}$ .

Now that we have a consistent model for the correlation length, we incorporate this model into a  $\chi^2$  goodness of fit measure. We use subscripts 1 and 2 to indicate data sets for systems of size  $L_1$  and  $L_2$  being compared. We use  $L_2 = 2L_1$ . A general goodness of fit measure for quantifying how well two curves collapse in variables  $\rho$  vs.  $\omega$  starts with choosing a set of independent points  $\omega_k$  and at each point calculating the difference between  $\rho_1(\omega_k)$  and  $\rho_2(\omega_k)$ ,  $\Delta_{12}(\omega_k) = \rho_1(\omega_k) - \rho_2(\omega_k)$ .

For a  $\chi^2$  test with uncorrelated data this difference  $\Delta_{12}(\omega_k^0)$  at the point  $\omega_k^0$  would then be squared and normalized by the sum of the variances,  $\sigma_1^2(\omega_k^0)$  for the system of size  $L_1$  and  $\sigma_2^2(\omega_k^0)$  for the system of size  $L_2$ . This gives

$$\chi_0^2(d_s; L_1, L_2) = \sum_k \frac{\Delta_{12}^2(\omega_k^0)}{\sigma_1^2(\omega_k^0) + \sigma_2^2(\omega_k^0)}, \quad (16)$$

where we would sum over discrete points  $\omega_k^0$  chosen with uniform spacing [32].

To incorporate the correlations we’ve observed into our definition of  $\chi^2$ , we compare the spacing of points chosen for the sum with the correlation length. Specifically, we assume that if we choose points  $\omega_k$  logarithmically spaced, i.e.,  $\omega_{k+1} = q\omega_k$ , we will effectively have a constant scaled correlation length, for  $\omega_k \leq 1$ . And for some choice of  $q$  this scaled correlation length will be equal to 1, allowing us to use the form of Eq. (16):

$$\chi^2 = \sum_k \frac{\Delta_{12}^2(\omega_k)}{\sigma_1^2(\omega_k) + \sigma_2^2(\omega_k)}. \quad (17)$$

If we consider taking the continuum limit of this equa-

tion, we see that

$$\begin{aligned}\chi^2 &= \int \frac{\Delta_{12}^2}{\sigma_1^2 + \sigma_2^2} d(\log_q \omega) \\ &= \int \frac{\Delta_{12}^2}{\sigma_1^2 + \sigma_2^2} \left( \frac{1}{\ln(q)\omega} \right) d\omega \\ &\propto \int \frac{\Delta_{12}^2}{\ell_q(\sigma_1^2 + \sigma_2^2)} d\omega ,\end{aligned}\quad (18)$$

where we have defined  $\ell_q = \ln(q)\omega$ . If we revert back to the discrete form, we see that our generalized goodness of fit measure becomes

$$\chi^2 = \sum_k \frac{\Delta_{12}^2(\omega_k^0)}{\ell(\omega_k^0)[\sigma_1^2(\omega_k^0) + \sigma_2^2(\omega_k^0)]} ,\quad (19)$$

where  $\ell(\omega_k^0) \propto \ell_q$  is the scaled correlation length at point  $\omega_k^0$  [33]. Dividing by the scaled correlation length will effectively weight each scaled correlation length sized ‘‘box’’ of data points in the  $\chi^2$  sum as one independent data point.

For our analysis, all runs ( $N = 4 \times 10^6$  samples per system size) were split into  $N_b = 400$  uniform batches (histograms) of  $N/N_b = 10^4$  samples apiece. This was done in part because storing data for all  $4 \times 10^6$  samples was impractical and running the bootstrap analysis over samples individually would be too time consuming to be feasible. To determine a useful batch size, we ran some preliminary tests by varying the batch size and plotting scaling collapses like Fig. 4. We saw similar estimated values of  $d_s$  based on these collapses, independent of batch size. A batch size of 400 seemed balanced because it allowed for error bars of order  $1/\sqrt{N_b} \approx 5\%$ . As we have shown in Eq. (12), the form of correlations should be independent of batch size chosen.

### C. Extrapolation to $L = \infty$

Next we must consider exactly what region in  $s$  of the data we want to fit. We address lattice effects by examining a lower (small  $s$ ) data cutoff. The upper (large  $s$ ) cutoff is also considered due to low statistics (large uncertainties) for  $s \gg L^{d_s}$ , though in the end we find that no upper cutoff is necessary. To determine reasonable cutoffs, we examine how the measured  $\chi^2$  and  $d_s$  respond to changes in these cutoffs. A more detailed discussion is included in Appendix C. Once we’ve decided upon fair cutoffs, this collapse procedure is run  $N_b$  times (once for each batch of data for each pair of sizes  $L_1, L_2$  with  $L_2 = 2L_1$ ). Each time, the value of  $d_s$  for which  $\chi^2$  is minimized is found, giving  $N_b$  independent estimates  $d_s(\alpha, L_1, L_2)$  for a given pair of systems  $L_1$  and  $L_2$ . The final estimate of  $d_s$  for this pair of systems is the average of the  $N_b$  independent estimates:

$$\overline{d_s(L_1, L_2)} = \frac{1}{N_b} \sum_{\alpha=1}^{N_b} d_s(\alpha, L_1, L_2) .\quad (20)$$

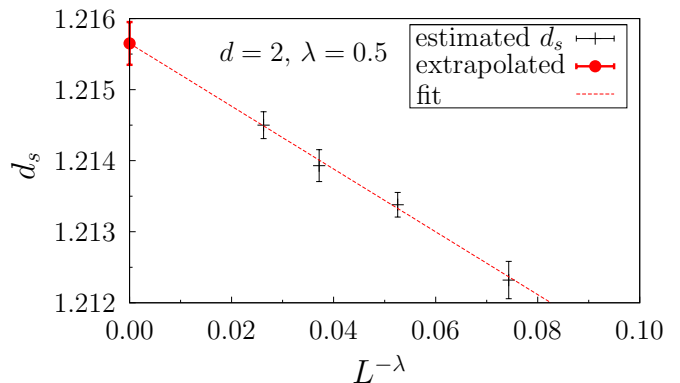


Figure 9: An illustration of a linear least squares fitting method being used to extract the value of  $d_s$  in the infinite system size limit in dimension  $d = 2$ . The fit uses the form  $d_s(L) = AL^{-\lambda} + d_s(\infty)$  where  $\lambda$  is a correction to scaling exponent and  $A$  and  $d_s(\infty)$  are fitting parameters. Here  $\lambda = 0.5$ , and  $L = \sqrt{L_1 L_2}$ , where  $L_1$  and  $L_2$  are the two system sizes used to produce a given data point. The fit found gives  $d_s(\infty) = 1.216(1)$ .

Then the sample variance  $S^2(L_1, L_2)$  in these  $N_b$  estimates is used to estimate the statistical error bars in the final estimate,

$$\sigma_{d_s}(L_1, L_2) = \frac{S(L_1, L_2)}{\sqrt{N_b - 1}} .\quad (21)$$

At this point we have obtained a single estimate of  $d_s$  (with error bars) for each consecutive pair of systems simulated.

Next we look to see if this  $\overline{d_s(L_1, L_2)}$  converges to some value as  $L_1$  and  $L_2$  tend to infinity. We extrapolate the infinite system size limit using a variety of least squares fitting routines adapted from the GNU Scientific Library [34]. Standard scaling suggests that  $d_s$  as a function of system size  $L$  will exhibit power law scaling behavior. But since we have no knowledge of the expected value for the exponent in this power law, we can allow this exponent to vary as a parameter in our fit, plotting  $\overline{d_s}$  vs.  $L^{-\lambda}$ , where we take  $L$  to be the geometric mean  $L = \sqrt{L_1 L_2}$ . Allowing  $\lambda$  to vary, fitting the data gives an estimate for  $d_s$  as well as the correction to scaling exponent  $\lambda$ . See Fig. 9 for an example of one extrapolation attempt, where  $\lambda$  is seen to be roughly 0.5 and linear least squares fitting for  $\overline{d_s}$  vs.  $L^{-\lambda}$  is used for the four largest system sizes in  $d = 2$  dimensions.

### D. Blind test for analysis method

To test this data analysis procedure, we applied the procedure to the similar problem of the uniform spanning tree (UST) in dimension  $d = 2$  [35]. Whereas a minimal spanning tree seeks to minimize the total weight of a tree that spans all the vertices of the lattice, a uniform spanning tree is simply any tree that spans the vertices

Table I:  $d_s$  calculated using MST algorithms

Dimension $d$	Two-step	Prim's (no trimming)
2	1.216(1)	1.216(1)
3	1.46(1)	1.46(1)
4	1.65(2)	1.66(2)
5	1.86(4)	1.86(4)

of the lattice, chosen with equal weight from all possible spanning trees. It can be thought of as a generalization of the minimal spanning tree problem to a system where all edges have the exact same weight. The reason for using this system as a test case for the analysis method is that one can examine  $r(s)$  data to look at  $d_s$  for paths on the UST, just as one would examine such paths on an MST. The analysis should be completely analogous, and we observed directly that the correlations in the  $r(s)$  data for the UST have a similar structure to that of the MST, allowing us to use the form of Eq. (15) for  $\ell$ . To ensure no bias in this test, one of us was not made aware of the nature of the system at the time of this test but was only given the prepared  $r(s)$  data on which to blindly run the analysis. The final result from this blind test, using a range of systems of size  $128^2$  to  $1024^2$ , was  $d_s = 1.2499(4)$  for the UST, which agrees well with the known exact result  $d_s = 5/4$  in two dimensions [36]. This provides confidence in the data analysis method.

#### IV. RESULTS

Table I displays our final numerical estimates for  $d_s$ . The values in dimensions  $d = 2$  and  $d = 3$  agree with previous results [37–40] and have error bars that are similar or smaller. Our result for  $d_s$  in dimension  $d = 4$  is a bit higher than the result 1.59(2) by Cieplak, Maritan, and Banavar [37]. The fractal dimensions computed from the two-step MTISC agree with those of the intermediate, untrimmed Prim's MTISC, to within our error estimates.

Our results for the path length dimension  $d_s$  can be directly compared with the  $\mathcal{O}(\epsilon = 6 - d)$  expansion of Jackson and Read. A graphical comparison of the data is shown in Fig. 10. Our results are not in conflict with the first order perturbation theory calculations. Some previous comparisons of  $\mathcal{O}(\epsilon)$  calculations with numerical results for disordered materials show differences of similar magnitude [41].

We investigate possible  $\mathcal{O}(\epsilon^2)$  calculations using nonlinear fitting routines adapted from the GNU Scientific Library [34] to fit  $d_s$  vs.  $\epsilon$ . Using a two parameter fit,

$$d_s = 2 + a\epsilon + b\epsilon^2, \quad (22)$$

and allowing  $a, b$  to vary, we find a chi-squared of 3.8 for two d.o.f., suggesting consistency with a quadratic fit to within our errors. For this fit, we find  $a = -0.142(8)$ ,

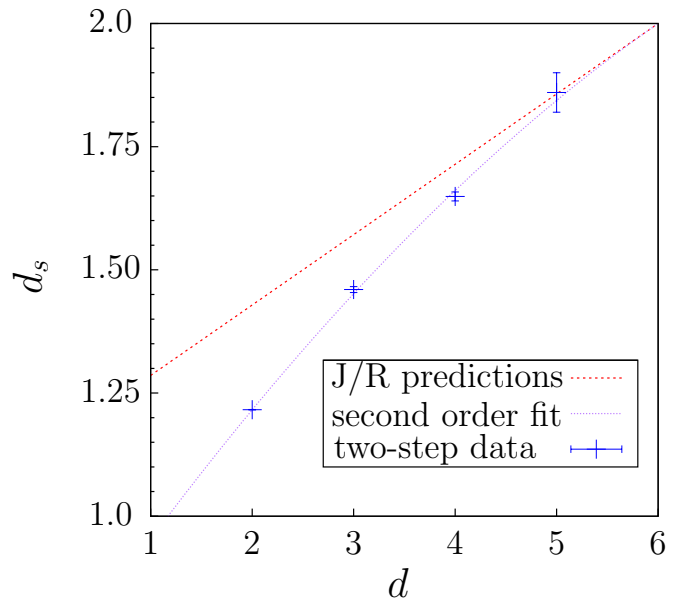


Figure 10: A plot comparing numerical results for  $d_s$  using the two-step method against predictions from the  $\mathcal{O}(\epsilon)$  perturbation expansion theorized by Jackson and Read. Also included is an example of a compatible  $\mathcal{O}(\epsilon^2)$  fit,  $d_s = 2 - \frac{\epsilon}{7} + b\epsilon^2$ , with a best fit value  $b = -0.0133$ .

which is near to the  $-1/7$  suggested by Jackson and Read. We find for this fit the value  $b = -0.014(2)$  for the second order prefactor.

Fixing  $a = -1/7$ , a one parameter fit,

$$d_s = 2 - \frac{\epsilon}{7} + b\epsilon^2, \quad (23)$$

gives  $b = -0.0133(1)$  with a chi-squared of 3.8 for three d.o.f. Presuming that the Jackson and Read result is correct to first order, this gives us a more precise numerical prediction for the second order term. This fit, Eq. (23), is plotted in Fig. 10.

#### V. SUMMARY

The intention of the two-step method was to allow the simulation of larger systems than were previously possible, reducing memory requirements of MST-finding algorithms by combining Prim's algorithm with Kruskal's algorithm. In this regard the work was successful, allowing for precise calculations of  $d_s$ . The trimming of the Prim's algorithm tree to possibly improve scaling of MTISCs constructed appears to have been unnecessary. Calculations using Prim's algorithm alone yielded almost identical results to those that used the two-step method.

We developed a data analysis method that allowed taking nonuniform correlations into account in order to obtain more accurate estimates for  $d_s$ . This analysis method should be applicable to a wide array of disordered systems with scale invariance and may be useful for future work.

The results for  $d_s$  calculated in this work are compatible with the perturbation expansion result proposed by Jackson and Read. Fitting  $d_s = 2 + a\epsilon + b\epsilon^2$ , we find  $a = -0.142(8)$ , compatible with the predicted  $a = -1/7$  [17]. Fixing the first order result to the Jackson and Read result, we used an  $\mathcal{O}(\epsilon^2)$  fit,  $d_s = 2 - \frac{\epsilon}{7} + b\epsilon^2$ , yielding  $b = -0.0133(1)$ . This could be checked if a higher order analytic calculation could be computed.

This work was made possible in part by NSF Grant No. DMR-1006731 and by the Syracuse University Gravitation and Relativity computing cluster, which is supported in part by NSF Grant No. PHY-0600953. This work was carried out largely using the Syracuse University HTC Campus Grid, a computing resource of approximately 2000 desktop computers supported by Syracuse University. Some of this work was discussed at the Aspen Center for Physics (NSF Grant No. 1066293).

## VI. APPENDIX

In this appendix, we present more precise definitions of the algorithms used to generate MTISCs, as well as details of the connection between  $T_P$ ,  $T_K$ , and  $T_2$ . We also discuss the region in  $s$  used for the  $\chi^2$  fitting procedure to estimate the fractal dimension  $d_s$ .

### A. Definitions and Algorithms

Here we present a more detailed discussion of Kruskal's and Prim's algorithms. We consider these MST-finding algorithms in the context of an undirected weighted graph  $G = (V, E, w)$ , where  $V$  is a set of vertices,  $E$  is a set of edges connecting these vertices, and we define a weight function  $w : E \mapsto \mathbb{R}$ , with each edge  $e \in E$  having weight  $w(e)$ . We consider the case of unique weights; no two edges in  $E$  have exactly the same weight.

In order to precisely describe the algorithms, it will be helpful to define some terms. A cycle or loop is a closed path such that the removal of any single edge from this path will result in the path becoming an open path, a connected set of edges with no vertex shared by more than two edges. When constructing trees, the notion of allowed and forbidden cycles is useful. Every cycle in the finite set  $\mathcal{C}$ , the set of all possible cycles for graph  $G$ , is chosen to belong to  $\mathcal{C}_F$  (the set of forbidden cycles) or  $\mathcal{C}_A$  (the set of allowed cycles), where  $\mathcal{C}_F \cup \mathcal{C}_A = \mathcal{C}$  and  $\mathcal{C}_F \cap \mathcal{C}_A = \emptyset$ . In a typical application on a periodic lattice, the allowed cycles correspond to loops that wrap around the lattice, while forbidden cycles correspond to non-wrapping loops that can be deformed, plaquette by plaquette, to a point. A set of two or more edges is considered connected if every edge in the set shares a vertex with at least one other edge in the set. A cluster  $T$  is set of connected edges and the vertices that these edges connect. A cluster may contain cycles, whereas a tree is an acyclic cluster.  $T_E$  denotes the set of edges

in the cluster and  $T_V$  denotes the set of vertices in the cluster.

Consider edge  $e = (u, v)$  where  $e \in E$  and  $u, v \in V$ . Adding  $e$  to a cluster  $T$  means that the edge set for the cluster,  $T_E$ , becomes  $T_E \cup \{e\}$ , and the set of vertices in the cluster,  $T_V$ , becomes  $T_V \cup \{u, v\}$ . A forbidden edge for a cluster  $T$  is an edge that, if added to  $T$ , would cause  $T$  to gain a forbidden cycle. An edge that is not a forbidden edge is an allowed edge. An allowed terminating edge for a cluster  $T$  is an allowed edge that, if added to  $T$ , would cause  $T$  to gain an allowed cycle (a wrapping loop). The addition of this allowed cycle will be used as the termination condition for both Kruskal's and Prim's algorithms, which are described below.  $\partial T$  is the set of adjacent edges for a cluster  $T$ , consisting of all edges that have one (but not both) endpoints in cluster  $T$ . As this set of edges forms a border or frontier on the outer regions of the cluster, we call  $\partial T$  the frontier of cluster  $T$ . The forbidden frontier of this cluster,  $\partial_F T$ , is the subset of the adjacent edges that are forbidden edges for  $T$ . The allowed frontier of this cluster,  $\partial_A T$ , is the subset of the adjacent edges that are allowed edges for  $T$ .

To examine an edge in Kruskal's or Prim's algorithm is to select this edge during a step of the algorithm and decide whether to accept or reject this edge into a cluster based on the conditions of the algorithm (usually dealing with the weight of the edge and whether this edge is allowed or forbidden for a particular cluster).

Next we will present Kruskal's and Prim's algorithms, step by step, using the notation we have outlined above.

#### Kruskal's Algorithm:

1. Sort  $E$  by increasing weight  $w$  to form a list of edges  $L$ .
2. Initialize each vertex in the graph to be its own tree, not connected to any other vertices and containing no edges.
3. Select the first (lowest weight) edge  $e = (u, v) \in L$ . Remove this edge from  $L$ . If  $e$  is a allowed edge, join into a single tree the tree containing  $u$  with the tree containing  $v$ , adding edge  $e$ . If  $e$  is a forbidden edge (that is, adding edge  $e$  to to the tree(s) containing its endpoints  $u$  and  $v$  would introduce a forbidden cycle), edge  $e$  is disregarded and not added to any trees. Edge  $e$  has now been examined.
4. Repeat step (3) until a allowed terminating edge, i.e., one that introduces an allowed (wrapping) cycle, is selected. The tree that contains both the vertices of this edge is identified as the Kruskal's MTISC  $T_K$ , and the allowed terminating edge that is examined in this final step is the Kruskal's wrapping edge,  $e_K \in E$ .

#### Prim's Algorithm:

1. Initialize the growing Prim's tree  $T_g$  to have one site, called the Prim's origin,  $v_0 \in V$ . Note that

$T_g$  is both a function of the  $v_0$  and time (number of iterations of Prim's algorithm), since  $T_g$  "grows" from the origin  $v_0$  by adding edges and vertices as Prim's algorithm proceeds.

2. Sort the frontier of the current Prim's tree,  $\partial T_g$ , by increasing edge weight  $w$  to form the Prim's queue (a function of  $T_g$ ), excluding any edges that have already been examined.
3. Select the first (lowest weight) edge  $e = (u, v)$  in the Prim's queue. If  $e$  is a allowed edge, add it to  $T_g$ , and if either  $u$  or  $v$  is not already in  $T_g$ , add it to  $T_g$  as well. Otherwise, if  $e$  is a forbidden edge, disregard the edge and do not add it to  $T_g$ . Edge  $e$  has now been examined.
4. Repeat steps (2)-(3) until a allowed terminating edge, i.e., one that introduces an allowed (wrapping) cycle, is selected. At this time, the growing Prim's tree  $T_g$  is identified as the Prim's MTISC  $T_P$ , and the allowed terminating edge examined in this final step is the Prim's wrapping edge,  $e_P(v_0) \in E$ . Note that  $T_P$  and  $e_P$  are both functions of the Prim's origin  $v_0$ .

### B. Proof of validity for two-step method

The two-step method first applies Prim's algorithm to find  $T_P \cup e_P$ . Kruskal's algorithm is then executed using the edges in  $T_P \cup e_P$ , serving as a trimming procedure for  $T_P$  and yielding what we will term the two-step MTISC,  $T_2$ . Here we will prove that the two-step method for MTISC generation yields  $T_2 = T_K$  in all cases except in the case of multiple disjoint ISCs. All results of this method can be divided into three cases. The first is the case where  $T_P$  is exactly equal to  $T_K$  and no trimming is needed, yielding  $T_P = T_2 = T_K$ . In the second case,  $T_K$  is a subset of  $T_P$ , and the trimming procedure of the two-step method yields  $T_2 = T_K$ . In the third case, there are multiple disjoint ISCs, and  $T_P$  and  $T_K$  share no common edges or vertices, meaning that  $T_2 \neq T_K$ . In other words, we will prove that

$$(T_P \supseteq T_K) \vee (T_P \cap T_K = \emptyset) \quad (\text{B.1})$$

and subsequently that  $T_2 = T_K$  in all cases except when the Prim's MTISC and the Kruskal's MTISC do not intersect. Here it will be useful to establish a few lemmas to aid in verifying these three cases we have outlined.

**Lemma 1** Edges in the allowed frontier of  $T_K$  have higher weight than edges in  $T_K$ .

**Proof** Because Kruskal's algorithm examines edges that are monotonically increasing in weight as the algorithm proceeds, at the time Kruskal's algorithm terminates, the edges that are not examined must be higher weight than

edges that have been examined. Since edges in the allowed frontier  $\partial_A T_K$  cannot be in  $T_K$ , this means that edges in  $T_K$  have been examined at the time of Kruskal's algorithm termination, whereas edges in  $\partial_A T_K$  have not. Thus edges in  $\partial_A T_K$  must be higher weight than edges in  $T_K$ .

**Lemma 2** For any given cycle  $c \in \mathcal{C}$  for which all edges of  $c$  are examined in Kruskal's algorithm, the edge in this cycle that is examined last must be the highest weight edge in this cycle.

**Proof** Because Kruskal's algorithm examines edges that are monotonically increasing in weight as the algorithm proceeds, for the finite set of edges in  $c$ , the highest weight edge in this set will be examined last in Kruskal's algorithm.

**Corollary 3** As a corollary, the Kruskal's wrapping edge  $e_K \in E$  has higher weight than any edge in the Kruskal's MTISC  $T_K$ .

**Proof** Because  $e_K$  is the last edge examined during the running of Kruskal's algorithm, it must have a weight higher than every other edge that is examined during the running of the algorithm, including every edge in  $T_K$ .

**Lemma 4** From lemma 2, for any edge  $e$  in the forbidden frontier of  $T_K$ , where adding  $e$  to  $T_K$  would form a forbidden cycle  $c_e$ ,  $e$  must be the highest weight edge in the forbidden cycle  $c_e$ .

**Proof** The criteria for an edge  $e$  to be in the forbidden frontier  $\partial_F T_K$  is that adding  $e$  to  $T_K$  would form a forbidden cycle  $c_e$ . This means that every edge in  $c_e \setminus \{e\}$  is in  $T_K$  and is examined before edge  $e$  during Kruskal's algorithm. Thus, edge  $e$  will have higher weight than any other edge in cycle  $c_e$ .

Using these lemmas that we have established, we will show that each realization of the two-step method can be categorized into one of three distinct cases, with cases 1 and 2 yielding  $T_2 = T_K$ . In the third case, we see that there are no common edges or vertices between  $T_P$  and  $T_K$ , so  $T_2 \neq T_K$  in this case.

**Case 1** If the Prim's origin  $v_0$  is a vertex in the Kruskal's MTISC  $T_K$ , then the Prim's MTISC  $T_P$  will be identical to the Kruskal's MTISC;  $T_P = T_K$ .

### Proof

Since Prim's algorithm grows a tree  $T_g$  by examining and adding edges adjacent to  $T_g$ , it will be crucial for us to pay close attention to the frontier of  $T_g$ ,  $\partial T_g$ . This frontier is sorted to form the Prim's queue from which edges are selected and considered for addition to  $T_g$ . In this first case, as long as we are only adding to  $T_g$  vertices that are also in  $T_K$ , the Prim's queue will consist entirely of

edges that are either in  $T_K$  or  $\partial T_K$ . The fulfillment of this condition,

$$\partial T_g \subseteq T_K \cup \partial T_K, \quad (\text{B.2})$$

will be shown in the remainder of the proof.

From lemma 1, when the frontier of the Prim's tree is sorted in Prim's algorithm to form the Prim's queue, any edges that are also in  $T_K$  will be placed before (having lower weight than) those edges in the allowed frontier of  $T_K$ . This means that all edges in  $T_K$  will be examined and added to  $T_g$  earlier in Prim's algorithm than edges in the allowed frontier of  $T_K$ . As the Prim's origin  $v_0$  is in  $T_K$ , we are guaranteed to have at least one edge from  $T_K$  added to the Prim's queue at the start of the Prim's growth. Furthermore, since  $T_K$  is connected, as edges from  $T_K$  are added to  $T_g$  through the Prim's growth, more edges from  $T_K$  and its frontier  $\partial T_K$  will be added to the Prim's queue, ensuring that  $T_g$  has more edges from  $T_K$  to add during further steps of Prim's algorithm.  $T_g$  begins as a single vertex  $v_0$  and grows to include more and more edges and vertices from  $T_K$  as Prim's algorithm proceeds.

Though we have shown that edges in  $T_K$  will be examined during Prim's algorithm before any edges in the allowed frontier of  $T_K$ , we cannot say the same about edges in its forbidden frontier,  $\partial_F T_K$ , which may also be in the Prim's queue and in consideration for selection during the Prim's growth. If edge  $x = (a, b) \in \partial_F T_K$  is in the Prim's queue, from lemma 4 we know that both vertices  $a$  and  $b$  are in  $T_K$ . If we call  $c_x$  the forbidden cycle that would be created in  $T_K$  by adding edge  $x$  to  $T_K$ , we also know from lemma 4 that  $x$  has higher weight than every other edge in the forbidden cycle  $c_x$ .

Thus, all edges in  $c_x \setminus \{x\}$  will be examined in Prim's algorithm and added to  $T_g$  before  $x$  is examined. So when  $x$  is finally examined in Prim's algorithm,  $x$  will be a forbidden edge for  $T_g$  and will not be added to  $T_g$ . This ensures that any forbidden cycles for  $T_K$  will be handled in the same manner in both Kruskal's and Prim's algorithms; no edges in the forbidden frontier of  $T_K$  will be added to  $T_g$ .

Using corollary 3, we can see that until the Kruskal's wrapping edge  $e_K$  is examined in Prim's algorithm, Eq. (B.2) will remain satisfied and all of the edges and vertices in  $T_K$  will be added to  $T_g$  before  $e_K$  is examined. Furthermore, as we have shown, none of the edges (allowed or forbidden) in the frontier of  $T_K$  will be added to the growing Prim's tree  $T_g$  before the Kruskal's wrapping edge  $e_K$  is examined. In this case,  $e_K$  will also serve as the Prim's wrapping edge  $e_P$ . Since the condition (B.2) is satisfied at the time  $e_K = e_P$  is examined in Prim's algorithm (terminating the algorithm by adding an allowed cycle),  $T_P = T_K$ . In this case, the Kruskal's trimming step of the two-step method is unnecessary, and the two-step method will yield  $T_2 = T_K$ .

**Case 2** If the Prim's origin  $v_0$  is not in the Kruskal's MTISC  $T_K$  but the Prim's tree  $T_g$  "grows" to include any vertices of  $T_K$ , then the Prim's MTISC  $T_P$  will include all of the Kruskal's MTISC  $T_K$ , i.e.,  $T_P \supset T_K$ .

### Proof

If we start Prim's algorithm from an origin  $v_0$  that is not a vertex in the Kruskal's MTISC  $T_K$ , we can define bridge edge  $b = (u_b, v_b)$  as the first edge added to the growing Prim's tree  $T_g$  that introduces a vertex of  $T_K$  into  $T_g$ . So  $b = (u_b, v_b)$  is the first edge added to  $T_g$  for which either  $u_b$  or  $v_b$  are in  $T_K$ .

At the point in Prim's algorithm when  $b$  is added to  $T_g$ ,  $b$  has a weight lower than any edge in the Prim's queue. Otherwise, edge  $b$  would not have been selected for addition to the Prim's tree at that time.

Examining edge  $b$  in the frame of the Kruskal's MTISC  $T_K$ , we know that edge  $b$  is in the allowed frontier of  $T_K$  since only one of  $u_b$  or  $v_b$  is in  $T_K$ . This means that  $b$  cannot be in  $T_K$  itself, nor can  $b$  be in the forbidden frontier of  $T_K$ . Because  $b$  is in the allowed frontier of  $T_K$ , it has a weight higher than any edge in  $T_K$ , by lemma 1. Thus, Prim's algorithm will continue as in case 1, with growth continuing from this first vertex of  $T_K$  (either  $u_b$  or  $v_b$ ) that is introduced to  $T_g$ . Any edges from  $T_K$  that are added to the Prim's queue will be added to the front (lower weight end) since these edges will all have a weight lower than  $w(b)$ , whereas every edge in the Prim's queue thus far has weight higher than  $w(b)$ .

Prim's algorithm will add edges from the Kruskal's MTISC  $T_K$  until reaching termination with the examination of the Kruskal's wrapping edge  $e_K$ , which in this case will also be the Prim's wrapping edge  $e_P$ . At this point  $T_P \supset T_K$ . In this case, the Kruskal's algorithm portion of the two-step method will serve to trim from the Prim's tree the region near the origin  $v_0$  up to the bridge  $b$ , leaving  $T_2 = T_K$ .

**Case 3** If the Prim's origin  $v_0$  is not in the Kruskal's MTISC  $T_K$  and the growing Prim's tree  $T_g$  does not "grow" to include any vertices of  $T_K$  before Prim's algorithm terminates, then the Prim's MTISC and the Kruskal's MTISC will not intersect. In other words,  $T_P \cap T_K = \emptyset$ .

### Proof

In this case, during Prim's algorithm, the Prim's wrapping edge  $e_P$  is examined before any vertices of the Kruskal's MTISC  $T_K$  are examined or added to the Prim's tree. The algorithm terminates with  $T_P \cap T_K = \emptyset$ . In this case, the two-step method will yield  $T_2 \neq T_K$ . However, this case is uncommon, and it is seen by direct observation that  $T_2$  and  $T_K$  have similar scaling properties.

Taking all three cases for the two-step method, we can say that either the Prim's MTISC  $T_P$  contains or

is equal to the Kruskal's MTISC  $T_K$ , or the Prim's and Kruskal's MTISCs do not intersect. Symbolically,  $(T_P \supseteq T_K) \vee (T_P \cap T_K = \emptyset)$ . In cases 1 and 2, where  $T_P$  and  $T_K$  do overlap, the two-step MTISC  $T_2$  will be equal to the Kruskal's MTISC  $T_K$ . So in these cases the two-step method yields the same result as that obtained from running Kruskal's algorithm on the entire graph  $G$ . We see that  $T_2 = T_K$  in all cases except the case of multiple disjoint ISCs, where the Prim's MTISC  $T_P$  (and by construction the two-step MTISC  $T_2$  as well) does not intersect with the Kruskal's MTISC  $T_K$ .

### C. Fitting region for $\chi^2$

Here we will discuss the data cutoffs we impose in order to restrict exactly what region in  $s$  of data we want to fit. These data cutoffs allow us to reduce overfitting errors in our  $\chi^2$  fitting routine (Eq. (19)) for estimating the fractal dimension  $d_s$ . We consider a small  $s$  (lower) cutoff by implementing  $s_l$  as the minimum  $s$  value allowed into the fitted data. We also consider a large  $s$  (upper) data cutoff by enforcing an  $\omega_u$  as the maximum allowed value for any of the scaled data in the fit. Introducing an  $\omega_u$  cutoff seemed natural because  $\omega \gg 1$  corresponds to paths that are much longer than  $L^{d_s}$  and are rare. Since these long paths are less frequent, data points with a large  $\omega$  value have higher statistical uncertainties than those with smaller  $\omega$  values. For small  $s$  we consider lattice effects. It made sense to use  $s_l$  as a low cutoff since we have small discrete  $s$  values (steps) in the paths. Using  $\omega_l$  would also have been a viable option, but it is easier to interpret the physical meaning of  $s_l$ , since one unit of  $s$  corresponds to the lattice spacing for all system sizes.

To determine reasonable values to use for the upper and lower data cutoffs, we tested our  $\chi^2$  fitting routine with various values of these cutoffs and assessed how well the minimum value of  $\chi^2$  agreed with a predicted estimate  $\chi_p^2$ . To estimate  $\chi_p^2$ , it is instructive to envision comparing data sets from two different system sizes on scaled axes  $\rho$  vs.  $\omega$ , as in Fig. 5(a). We use a discrete set  $\{\omega_k^0\}$ , consisting of  $n$  uniformly spaced values of  $\omega$ , to calculate a set of  $\rho(\omega_k^0)$  values for each of the two data sets. The comparison between these  $\rho$  values goes into the calculation of  $\chi_2$ , as outlined in Eq. (19).

One can imagine breaking the  $\omega$  axis up into  $b$  segments or "boxes" of length equal to the scaled correlation length  $\ell$ . Each box will contain some number  $n_b$  of data points from the set of  $n$  points in the  $\{\omega_k^0\}$  discrete points we use to calculate the goodness of the collapse. In this way, we can estimate  $\chi_p^2$  piece by piece, calculating separately the contribution  $\chi_b^2$  from each of the  $b$  boxes:

$$\chi_p^2 = \chi_b^2 b. \quad (\text{C.1})$$

Further, we can estimate  $n_b$ , the number of data points that fall in each of these boxes. This allows us to subdivide the  $\chi_b^2$  into contributions from each individual data

point,  $\chi_1^2$ :

$$\chi_p^2 = \chi_1^2 n_b b. \quad (\text{C.2})$$

Now that we have partitioned  $\chi_p^2$  by this relation, we can calculate  $\chi_1^2$ ,  $n_b$ , and  $b$  individually. First, we can estimate  $\chi_1^2$ , the  $\chi^2$  contribution from a single data point in the set of  $\{\omega_k^0\}$  values, by its expectation value  $E(\chi_1^2)$ . We can write, using the form of Eq. (19),

$$\begin{aligned} \chi_1^2 &\approx E(\chi_1^2) \\ &\approx \frac{E([\rho_1 - \rho_2]^2)}{\ell[\sigma_1^2 + \sigma_2^2]} \\ &\approx \frac{E(\rho_1^2) + E(\rho_2^2)}{\ell[\sigma_1^2 + \sigma_2^2]} \\ &\approx \frac{\sigma_1^2 + \sigma_2^2}{\ell[\sigma_1^2 + \sigma_2^2]} \\ &\approx \frac{1}{\ell}, \end{aligned} \quad (\text{C.3})$$

where  $\rho_1(\rho_2)$  is the  $\rho$  value taken from data set 1(2), and  $\sigma_1^2(\sigma_2^2)$  is the variance at this point for data set 1(2).

Next we can write an expression for the number of data points per box,  $n_b$ , by multiplying the length of each box,  $\ell$ , by the density of data points,

$$n_b = \ell \left( \frac{n}{\omega_u - \omega_l} \right), \quad (\text{C.4})$$

where again  $n$  is the total number of data points in the set  $\{\omega_k^0\}$  being used for the  $\chi^2$  calculation and  $\omega_u - \omega_l$  gives the full allowed range of  $\omega_k^0$  values.

Finally, we compute the total number  $b$  of boxes,  $b$ , by dividing the range  $\omega_u - \omega_l$  into two regions,  $\omega < 1$  and  $\omega > 1$ . This allows us to separately compute the number of boxes in each of these regions,  $b_<$  and  $b_>$  respectively. Of course,  $b = b_< + b_>$ . Expressing  $b_>$  is trivial, since in this region the scaled correlation length is constant at  $\ell = A$  (as given by our model in Eq. (15)), where  $A$  is the proportionality constant relating  $\ell$  and  $\omega$  by  $\ell = A\omega$ . Thus we write

$$b_> = \frac{\omega_u - 1}{A}. \quad (\text{C.5})$$

Writing  $b_<$  is not quite as simple. It may help to begin at  $\omega = 1$  and think of stepping left toward lower values of  $\omega$  and eventually to  $\omega_l$ , counting up the number of boxes we step across. The boundary of the first box will occur at  $\omega = (1 - A)$ , since the scaled correlation length  $\ell$  is equal to  $A$  around  $\omega = 1$ . Likewise, the edge of the second box we approach will fall at  $\omega = (1 - A)^2$ , the  $i^{\text{th}}$  box will reach to  $\omega = (1 - A)^i$ , and the final  $b_<^{\text{th}}$  box will fall at the lowest allowed  $\omega$  value,  $\omega_l$ . So we can write

$$\omega_l = (1 - A)^{b_<}, \quad (\text{C.6})$$

from which it follows that

$$\begin{aligned} b_< &= \frac{\ln(\omega_l)}{\ln(1 - A)} \\ &\approx \frac{\ln(1/\omega_l)}{A}. \end{aligned} \quad (\text{C.7})$$

Here an approximation is made in the denominator since  $A$  is small.

Combining Eqs. (C.2), (C.3), (C.4), (C.5), and (C.7), we can write an expression for  $\chi_p^2$  by adding the contributions from both of the two regions we examined,  $\omega < 1$  and  $\omega > 1$ :

$$\begin{aligned} \chi_p^2 &= \frac{1}{\ell} \left[ \ell \left( \frac{n}{\omega_u - \omega_l} \right) \right] \left[ \frac{\ln(1/\omega_l)}{A} \right] \\ &+ \frac{1}{\ell} \left[ \ell \left( \frac{n}{\omega_u - \omega_l} \right) \right] \left[ \frac{\omega_u - 1}{A} \right] \\ &= \frac{1}{A} \left[ \frac{n}{\omega_u - \omega_l} \right] \left[ \ln \left( \frac{1}{\omega_l} \right) + \omega_u - 1 \right]. \end{aligned} \quad (\text{C.8})$$

In general, this proportionality constant  $A$  will depend on what method is used to measure correlation length.

For this reason, we look at the ratio  $\chi_p^2/\chi^2$ . Since both  $\chi_p^2$  and  $\chi^2$  have a  $1/A$  dependence, the ratio of the two is independent of  $A$ .

We use this ratio  $\chi_p^2/\chi^2$  to get an idea of the effect various upper and lower data cutoffs have on our fit. We plot an example case of this analysis for systems of size  $L = 512$  and  $L = 1024$  in dimension  $d = 2$ . In Figs. 11(a) and 11(b) it is apparent that below a certain  $s_l$  threshold, lattice effects skew the value of  $\chi^2$  as well as the value of  $d_s$ . Meanwhile, Figs. 11(c) and 11(d) indicate that we need not impose an upper cutoff on the data. The high variance of points in the large  $\omega$  region of the data already appropriately weights these points. For our final analysis, we chose  $s_l = 425$  for two dimensions,  $s_l = 375$  for three dimensions, and  $s_l = 100$  for four and five dimensions.

- 
- [1] T. H. Cormen, C. Stein, R. L. Rivest, and C. E. Leiserson, *Introduction to Algorithms*, 2nd ed. (MIT Press, Cambridge, MA, USA, 2001).
- [2] E. W. Dijkstra, *Numerische Mathematik* **1**, 269 (1959).
- [3] V. Petäjä, M. Sarjala, M. Alava, and H. Rieger, *Phys. Rev. B* **73**, 094517 (2006).
- [4] D. A. Huse and C. L. Henley, *Phys. Rev. Lett.* **54**, 2708 (1985).
- [5] H. Luo *et al.*, *Physics Letters A* **250**, 383 (1998).
- [6] A. A. Middleton, *Phys. Rev. B* **61**, 14787 (2000).
- [7] A. C. Carter, A. J. Bray, and M. A. Moore, *Phys. Rev. Lett.* **88**, 077201 (2002).
- [8] E. Fehr *et al.*, *Phys. Rev. E* **84**, 036116 (2011).
- [9] C. M. Newman and D. L. Stein, *Phys. Rev. Lett.* **72**, 2286 (1994).
- [10] R. C. Prim, *Bell Syst. Tech. J.* **36**, 1389 (1957).
- [11] W. Chou and A. Kershenbaum, in *Proceedings of the third ACM symposium on Data communications and Data networks: Analysis and design, DATACOMM '73* (ACM, New York, NY, USA, 1973), pp. 148–156.
- [12] H. Loberman and A. Weinberger, *J. ACM* **4**, 428 (1957).
- [13] A. W. F. Edwards and L. L. Cavalli-Sforza, *Systematics Association Publication*. **6**, 67 (1964).
- [14] R. Osteen and P. Lin, *SIAM Journal on Computing* **3**, 23 (1974).
- [15] T. T. Cormen, C. E. Leiserson, and R. L. Rivest, *Introduction to Algorithms* (MIT Press, Cambridge, MA, USA, 1990).
- [16] T. S. Jackson and N. Read, *Phys. Rev. E* **81**, 021130 (2010).
- [17] T. S. Jackson and N. Read, *Phys. Rev. E* **81**, 021131 (2010).
- [18] S. R. Broadbent and J. M. Hammersley, *Proceedings of the Cambridge Philosophical Society* **53**, 629 (1957).
- [19] H. Frisch and J. Hammersley, *Journal of the Society for Industrial and Applied Mathematics* **11**, 894 (1963).
- [20] M. Aizenman, *Nuclear Physics B* **485**, 551 (1997).
- [21] M. Aizenman, *IMA Vol. Math. Appl.* **99**, 1 (1996).
- [22] D. Wilkinson and J. F. Willemsen, *Journal of Physics A: Mathematical and General* **16**, 3365 (1983).
- [23] J. Goodman, *Journal of Statistical Physics* **147**, 919 (2012).
- [24] M. Damron, A. Sapozhnikov, and B. Vgvlgyi, *Annals of Probability* **37**, 2297 (2009).
- [25] J. van den Berg, Y. Peres, V. Sidoravicius, and M. E. Vares, *Annales de l'Institut Henri Poincaré - Probabilité and Statistics = Probabilities and Statistics* **44**, 1173 (2008).
- [26] J. B. Kruskal, *Proc. Am. Math. Soc.* **7**, 48 (1956).
- [27] A.-L. Barabási, *Phys. Rev. Lett.* **76**, 3750 (1996).
- [28] J. Machta *et al.*, *Phys. Rev. Lett.* **75**, 2792 (1995).
- [29] G. Paul, R. M. Ziff, and H. E. Stanley, *Phys. Rev. E* **64**, 026115 (2001).
- [30] P. Grassberger, *Phys. Rev. E* **67**, 036101 (2003).
- [31] P. Duxbury and R. Dobrin, *Physica A: Statistical Mechanics and its Applications* **270**, 263 (1999).
- [32] W. H. Press, B. P. Flannery, S. A. Teukolsky, and W. T. Vetterling, *Numerical Recipes in C: The Art of Scientific Computing*, 1 ed. (Cambridge University Press, New York, NY, USA, 1988).
- [33] G. E. P. Box and D. A. Pierce, *Journal of the American Statistical Association* **65**, pp. 1509 (1970).
- [34] M. Galassi *et al.*, *Gnu Scientific Library Reference Manual*, 3 ed. (Network Theory Ltd., <http://www.gnu.org/software/gsl>, 2003).
- [35] N. Read, *Phys. Rev. E* **70**, 027103 (2004).
- [36] S. N. Majumdar, *Phys. Rev. Lett.* **68**, 2329 (1992).
- [37] M. Cieplak, A. Maritan, and J. R. Banavar, *Phys. Rev. Lett.* **76**, 3754 (1996).
- [38] S. V. Buldyrev, S. Havlin, E. López, and H. E. Stanley, *Phys. Rev. E* **70**, 035102 (2004).
- [39] A. P. Sheppard, M. A. Knackstedt, W. V. Pinczewski, and M. Sahimi, *Journal of Physics A: Mathematical and General* **32**, L521 (1999).
- [40] B. Wieland and D. B. Wilson, *Phys. Rev. E* **68**, 056101 (2003).
- [41] K. Dahmen and J. P. Sethna, *Phys. Rev. Lett.* **71**, 3222 (1993).

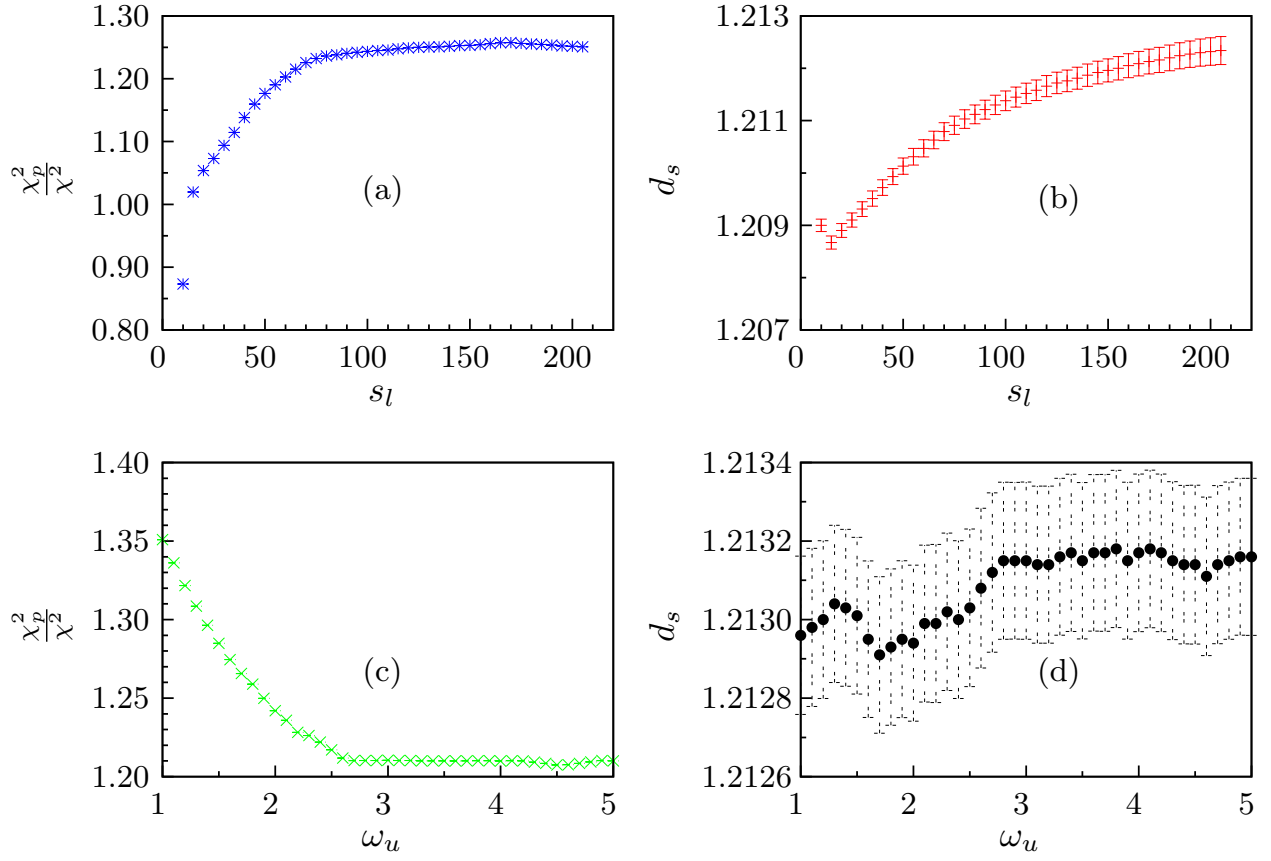


Figure 11: Examining the effects of the lower and upper data cutoffs on a collapse of two systems of sizes  $L = 512$  and  $L = 1024$  in dimension  $d = 2$ . (a) and (b) display  $\chi_p^2/\chi^2$  and  $d_s$  as functions of the lower (small  $s$ ) data cutoff  $s_l$ , while (c) and (d) show  $\chi_p^2/\chi^2$  and  $d_s$  as functions of the upper (large  $s$ ) data cutoff  $\omega_u$  for  $s_l = 100$ . Both  $\chi_p^2$  and  $\chi^2$  are measured at the value of  $d_s$  for which  $\chi^2$  is minimized.